

Efficient Reinforced DAG Learning without Acyclicity Constraints

Bao Duong, Hung Le, and Thin Nguyen

Applied Artificial Intelligence Institute, Deakin University, Australia
{b.duong,thai.le,thin.nguyen}@deakin.edu.au

Abstract

Unraveling cause-effect structures embedded in mere observational data is of great scientific interest, owing to the wealth of knowledge that can benefit from such structures. Recently, reinforcement learning (RL) has emerged as the enhancement for classical techniques to search for the most probable causal explanation in the form of a directed acyclic graph (DAG). Yet, effectively exploring the DAG space is challenging due to the vast number of candidates and the intricate constraint of acyclicity. In this study, we present **REACT** (**RE**inforced **DAG** learning without acyclicity **C**onstrain**T**s)—a novel causal discovery approach fueled by the RL machinery with an efficient DAG generation policy. Through a novel parametrization of DAGs, which allows for directly mapping a real-valued vector to an adjacency matrix representing a valid DAG in a single step without enforcing any acyclicity constraint, we are able to navigate the search space much more effectively with policy gradient methods. In addition, our comprehensive numerical evaluations on a diverse set of both synthetic and real data confirm the effectiveness of our method compared with state-of-the-art baselines.

1 Introduction

The knowledge of causal relationships offers the power to forecast possible consequences of interventions or even imagine alternative outcomes of counterfactuals, which are immensely valuable in many scientific sectors such as bioinformatic [Sachs *et al.*, 2005], econometric [Hünermund and Bareinboim, 2023], and neural science [Cao *et al.*, 2019]. This has consequently motivated the development of causal discovery methods that aim to infer cause-effect relationships from purely passive data in the last decades.

Causal discovery is typically formulated as finding the directed acyclic graph (DAG) representing the causal model that most likely generated the observed data. Among the broad literature, score-based methods are one of the most well-recognized approaches. The core idea is to give each possible DAG \mathcal{G} a “score” $\mathcal{S}(\mathcal{D}, \mathcal{G})$ that quantifies how much

Table 1: Conceptual comparison between the proposed method with RL-related methods. To enforce acyclicity, RL-BIC [Zhu *et al.*, 2020] incorporates a soft DAG regularization to the reward, while CORL [Wang *et al.*, 2021], GARL [Yang *et al.*, 2023b], RCL-OG [Yang *et al.*, 2023a], and DAG-GFN [Deleu *et al.*, 2022] explicitly identify and mask out the actions that lead to cycles.

Method (year)	Search space	Generation cost	Constraint	Acyclicity assurance
RL-BIC (2020)	Graphs	One-step	Soft	✗
CORL (2021)	Orderings	Multiple-step	Hard	✓
DAG-GFN (2022)	DAGs	Multiple-step	Hard	✓
GARL (2023)	Orderings	Multiple-step	Hard	✓
RCL-OG (2023)	Orderings	Multiple-step	Hard	✓
REACT (Ours)	DAGs	One-step	None	✓

it can explain the observed data \mathcal{D} , and then search for the DAG possessing the best score: $\mathcal{G}^* = \arg \min_{\mathcal{G}} \mathcal{S}(\mathcal{D}, \mathcal{G})$ s.t. $\mathcal{G} \in \text{DAGs}$. Solving this optimization problem is generally NP-hard [Chickering, 1996], due to the *huge search space* that grows super-exponentially with the number of variables [Robinson, 1977] and the *intricate acyclicity constraint*. Most methods therefore resort to local heuristics, such as GES [Chickering, 2002] which gradually adds edges into the graph one-by-one while actively maintaining acyclicity. With the introduction of soft DAG characterizations [Zheng *et al.*, 2018; Yu *et al.*, 2019; Zhang *et al.*, 2022], the combinatorial optimization problem above can be turned into a continuous optimization problem, allowing for more effectively exploring the DAG space, as multiple edges can be added or removed simultaneously in an update.

Despite the advent of continuous optimization methods, the global optimality of the solution is unlikely achieved due to the local heuristic nature of the optimization strategies. This gives rise to the adaptation of reinforcement learning (RL) into score-based causal discovery [Zhu *et al.*, 2020; Wang *et al.*, 2021; Yang *et al.*, 2023a,b] as the improved search strategy, thanks to its exploration and exploitation abilities. Zhu *et al.* [2020] initially propose an actor-critic agent that learns to generate good-scoring graphs, with the acyclicity handled by fusing the soft DAG regularization from Zheng *et al.* [2018] into the reward. Unfortunately, the approach may not prohibit all cycles and potentially waste time for exploring non-DAGs. To overcome this, ordering-based RL methods [Wang *et al.*, 2021; Yang *et al.*, 2023a,b] instead

search for high-reward *causal orderings*, where a cause always precedes its effects, then apply variable selection to obtain DAGs. On a similar note, deviating slightly from RL-based methods, Deleu *et al.* [2022] introduce a Bayesian DAG learning method which generate DAGs by adding edges one-by-one with explicit exclusions of cycle-inducing edges, and the edge addition probabilities are learned via flow-matching objectives [Bengio *et al.*, 2023]. However, the orderings and DAGs in these methods are constructed in a sequential manner, which hinders parallel DAG generation and necessitates learning the transition policies over a multitude of discrete state-action combinations. For instance, the complexity for generating a single ordering element in CORL [Wang *et al.*, 2021] is already quadratic in the number of nodes, totaling a cubic runtime since the generations of all elements cannot be done simultaneously.

In this study, we address the aforementioned limitations of score-based and ordering-based causal discovery methods with a novel RL approach, named **REACT** (**R**Einforced **D**AG learning without acyclicity **C**onstrain**T**s). Our approach employs a generative policy that is capable of generating DAGs in a single-step fashion without any acyclicity regularization nor explicit acyclicity maintenance. This one-step generation costs only a quadratic number of parallel operations w.r.t. the number of nodes, allowing us to effectively explore and exploit the full DAG space rather than the restricted ordering space (see Table 1 for a clear comparison between our method and other RL-related approaches). The main contributions in our study are summarized as follows:

1. At the core of **REACT**, we design **Vec2DAG**, a *surjective map* from a continuous domain into the space of all DAGs. We prove that given a fixed number of nodes, this function can translate an unconstrained real-valued vector into a binary matrix that represents a valid DAG, and vice versa—there always exists a vector mapped to every possible DAG.
2. Thanks to **Vec2DAG**, we are able to devise a policy outputting actions in the continuous domain that are directly associated with high-reward DAGs. The policy is one-step and unconstrained, allowing our causal discovery agent **REACT** to explore the DAG space very effectively. To our knowledge, **REACT** is the first RL-based method that can explore the exact space of DAGs with an efficient one-step generation.
3. We demonstrate the effectiveness of the proposed **REACT** method in comparison with various state-of-the-arts on a systematic set of numerical evaluations of both synthetic and real-world datasets. Empirical results show that our method consistently surpasses all state-of-the-art baselines under multiple evaluation metrics on synthetic data and achieves competitive performance on real data, while having a much faster runtime compared with RL-based competitors.

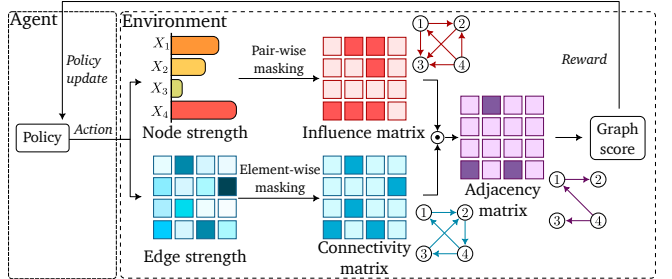


Figure 1: Schematic overview of **REACT** in case there are four variables. The agent tries to learn an optimal policy to generate high-reward DAG representations, i.e., action vectors. To produce DAGs, we decompose the action vector into a node strength vector and an edge strength matrix. The node strength vector is then transformed into an “influence matrix” where only stronger nodes can influence weaker nodes, thus prohibiting all cycles. Meanwhile, the edge strength matrix produces a “connectivity matrix” where only sufficiently strong edges are kept. Next, these matrices are combined via the Hadamard product, leaving us with only edges that appear in both matrices, which are guaranteed to be DAGs. Finally, the scoring of how much the resultant DAG fits the observed data is used to derive the reward to train the agent’s policy.

2 Background

2.1 Functional Causal Model

Let $\mathbf{X} = (X_1, \dots, X_d)$ be the d -dimensional random vector representing the variables of interest, $\mathbf{x}^{(k)} = (x_1^{(k)}, \dots, x_d^{(k)}) \in \mathbb{R}^d$ denotes the k -th observation of \mathbf{X} , and $\mathcal{D} = \{\mathbf{x}^{(k)}\}_{k=1}^n$ indicates the observational dataset containing n samples of \mathbf{X} . Assuming *causal sufficiency*, that is, there are no unobserved endogenous variables, the causal structure among said variables can be described by a DAG $\mathcal{G} = (\mathcal{V}, \mathcal{E})$ where each vertex $i \in \mathcal{V} = \{1, \dots, d\}$ corresponds to a random variable X_i , and each edge $(j \rightarrow i) \in \mathcal{E}$ implies that X_j is a direct cause of X_i . We also denote the set of all direct causes of a variable as its *parents*, i.e., $\text{pa}_i = \{j \in \mathcal{V} \mid (j \rightarrow i) \in \mathcal{E}\}$. The DAG \mathcal{G} is also represented algebraically with a binary *adjacency matrix* $\mathbf{A} \in \{0, 1\}^{d \times d}$ where the (i, j) -th entry is 1 if $(i \rightarrow j) \in \mathcal{E}$ and 0 otherwise. To formalize the causal mechanisms that dictate how causes influence effects, we follow Zhu *et al.* [2020]; Wang *et al.* [2021]; Yang *et al.* [2023a,b] to assume additive noise causal models (ANM) [Hoyer *et al.*, 2008] as the data generation process as follows:

$$X_i := f_i(\mathbf{X}_{\text{pa}_i}) + E_i, \quad i = 1, 2, \dots, d, \quad (1)$$

where the noises E_i are mutually independent. In addition, we also assume *causal minimality* [Peters *et al.*, 2014], implying that each function f_i is non-constant to any of its arguments. The goal of causal discovery is then to recover the acyclic graph \mathcal{G} from the data induced by Eqn. (1).

Furthermore, we only consider identifiable models for the simplicity of evaluating the correctness of the estimated DAG with respect to the ground truth DAG. The linear-Gaussian model with the introduction of the equal-variance assumption is an example of this class of models [Peters *et al.*, 2014].

Moreover, nonlinear ANMs are typically identifiable, since the space of parameters rendering unidentifiability is strictly limited to a three-dimensional affine space [Hoyer *et al.*, 2008]. Nevertheless, extensions of our method to more advanced settings are relatively straightforward, provided with properly designed score functions.

A comprehensive review of related works in causal discovery can be found in Appendix A.

2.2 DAG Scoring

Among multiple DAG scoring functions well-developed in the literature, here we focus on the popular BIC score [Schwarz, 1978], which is adopted in many works for its simplicity and theoretical soundness. Specifically, for additive Gaussian noises with potentially non-equal noise variances, the BIC can be specified as follows

$$S_{\text{BIC}}(\mathcal{D}, \mathcal{G}) = n \sum_{i=1}^d \ln \frac{\text{SSR}_i}{n} + |\mathcal{G}| \ln n + \text{const}, \quad (2)$$

where $\text{SSR}_i = \sum_{k=1}^n (\hat{x}_i^{(k)} - x_i^{(k)})^2$ is the sum of squared residuals after regressing X_i on its parents in \mathcal{G} .

Additionally assuming equal noise variances gives us with

$$S_{\text{BIC}}(\mathcal{D}, \mathcal{G}) = nd \ln \frac{\sum_{i=1}^d \text{SSR}_i}{nd} + |\mathcal{G}| \ln n + \text{const}. \quad (3)$$

The derivations of Eqn. (2) and Eqn. (3) are presented in Appendix B.3.

2.3 DAG Sampling

Generating DAGs from a parametrized distribution is essential for learning in the DAG space. To handle acyclicity, most methods rely on a well-known decomposition of a DAG into two binary matrices:

$$\mathbf{A} = \boldsymbol{\Pi}^\top \mathbf{U} \boldsymbol{\Pi} \quad (4)$$

where $\boldsymbol{\Pi} \in \{0, 1\}^{d \times d}$ is a permutation matrix and $\mathbf{U} \in \{0, 1\}^{d \times d}$ is a strictly upper-triangular matrix. Simply put, \mathbf{U} represents the adjacency matrix of a graph containing only edges $(j \rightarrow i)$ with $j < i$, effectively discarding all cycles. Then, the permutation matrix $\boldsymbol{\Pi}$ simply rearranges the node labels in this DAG, resulting in another graph with identical topology, i.e., acyclicity assured.

To explore the DAG space, Eqn. (4) suggests exploring the causal ordering space and then applying variable selection to remove unneeded edges, which is naturally a common approach for ordering-based algorithms. That being said, generating permutations poses a significant problem in many methods [Cundy *et al.*, 2021; Wang *et al.*, 2021; Charpentier *et al.*, 2022; Yang *et al.*, 2023b,a] regarding computational efficiency. For example, in ordering-based RL methods [Wang *et al.*, 2021; Yang *et al.*, 2023b,a], the generation of permutations is formulated as a Markov decision process, so the cost of generating a single element, which is usually at least $\mathcal{O}(d^2)$ due to the use of Transformer-based policies, adds up to $\mathcal{O}(d^3)$ for generating a single ordering, which can increase

depending on the variable selection technique employed to turn the ordering to a DAG.

Alternatively, *differentiable DAG sampling* schemes based on Eqn. (4) have also been proposed by Charpentier *et al.* [2022] and Cundy *et al.* [2021]. The permutation matrices in their methods are generated by either applying many iterations of the Sinkhorn operator [Sinkhorn, 1964] followed by the Hungarian algorithm [Kuhn, 1955] with a considerable cost of $\mathcal{O}(d^3)$, or sorting score vectors of size d if a combination of Gumbel-Top- k trick [Kool *et al.*, 2019] and SoftSort operator [Prillo and Eisenschlos, 2020] is used.

On a related note, *unconstrained DAG representations* have also been proposed [Yu *et al.*, 2021; Massidda *et al.*, 2024], however they are more focused in the context of *continuous optimization*, with special treatments to ensure differentiability. More particularly, the DAG characterization from Yu *et al.* [2021], i.e., $\mathbf{A} = \mathbf{W} \odot \text{ReLU}(\text{grad}(\mathbf{p}))$ where $\text{grad}(\mathbf{p})_{ij} = p_j - p_i$, represents a weighted adjacency matrix of a DAG, which is only valid for linear models. Moreover, this representation is only used as a refinement for the result returned by a constrained optimization problem. Meanwhile, the soft DAG parameterization by Massidda *et al.* [2024], where $\mathbf{A} = \mathbf{W} \odot \text{sigmoid}(\text{grad}(\mathbf{p})/\tau)$, only ensures acyclicity at the limit of the annealing temperature $\tau \rightarrow 0^+$.

3 REACT: Efficient Reinforced DAG Learning without Acyclicity Constraints

The core idea of our method is to find a deterministic translation from an unconstrained continuous space to the space of DAGs, which would allow us to search in the surrogate space freely with no constraints instead of navigating directly in the DAG space while avoiding cycles. Then, instead of employing continuous optimization methods, which may stuck at a local optimum, we employ RL to elevate the chance of reaching the global optimum. Here in this section, we elaborate on how to define such a map and how to combine it with RL to create an efficient DAG learning algorithm. An illustrative overview of our method can be found in Figure 1.

3.1 Vec2DAG: Unconstrained Parameterization of DAGs

Contrary to the DAG generation approaches inspired by the permutation-based disentanglement in Eqn. (4), in this study, we instead adopt a different decomposition of DAGs that circumvents the challenging permutation generation problem. More specifically, our DAG representation is inspired by Yu *et al.* [2021] and involves an influence matrix and connectivity matrix as defined below

Definition 1. (*Influence matrix*). A matrix $\mathbf{C} \in \{0, 1\}^{d \times d}$ is an influence matrix if there exists a permutation matrix $\boldsymbol{\Pi} \in \{0, 1\}^{d \times d}$ such that

$$\mathbf{C} = \boldsymbol{\Pi}^\top \mathbf{T} \boldsymbol{\Pi}, \quad (5)$$

where $\mathbf{T} \in \{0, 1\}^{d \times d}$ is a strictly upper-triangular matrix where every entry above the main diagonal is 1.

An influence matrix therefore represents a complete DAG where no more edge can be added without introducing a cycle, and the node ordering is arranged by the permutation matrix Π . While the permutation matrix specifies the position a node should be placed in a causal ordering, our influence matrix determines if a node is a potential ancestor of another, and thus can “influence” it in a directed causal pathway. That is, the (i, j) -th entry being 1 indicates that i can influence j , but not vice versa.

Definition 2. (*Connectivity matrix*). A matrix \mathbf{E} is a connectivity matrix if it is a square binary matrix.

Our connectivity matrix serves a similar role to the aforementioned upper-triangular matrix \mathbf{U} , except that no restriction is imposed onto it. Given these matrices, the DAG decomposition in this study is theoretically grounded by our following Theorem:

Theorem 1. Let $\mathbf{A} \in \{0, 1\}^{d \times d}$ be the adjacency matrix associated with an arbitrary DAG. The adjacency matrix \mathbf{A} always admits a decomposition

$$\mathbf{A} = \mathbf{C} \odot \mathbf{E}, \quad (6)$$

where $\mathbf{C} \in \{0, 1\}^{d \times d}$ is an influence matrix, $\mathbf{E} \in \{0, 1\}^{d \times d}$ is a connectivity matrix, and \odot is the Hadamard (element-wise) product operator.

Proof. See Appendix B.1. \square

This decomposition is more computationally friendly compared to Eqn. (4) in terms of arithmetic operations, inspiring our method to generate a DAG by simulating a pair of influence and connectivity matrices. Regarding the former, Eqn. (5) may give the impression that in order to build an influence matrix, we must first produce a permutation matrix, which revolves back to existing ordering-based techniques. However, our next Lemma shows a promising alternative to efficiently sample an influence matrix without generating a permutation.

Lemma 1. Let $\mathbf{C} \in \{0, 1\}^{d \times d}$ be an influence matrix. Then, there always exists a vector $\mathbf{c} \in \mathbb{R}^d$ such that

$$C_{ij} = \begin{cases} 1 & \text{if } c_i > c_j \\ 0 & \text{otherwise} \end{cases} \quad (7)$$

Proof. See Appendix B.2. \square

On the other hand, any real-valued vector $\mathbf{c} \in \mathbb{R}^d$, excluding the rare cases of ties with measure zero, can define an influence matrix. Here in this work, we refer to \mathbf{c} as the “node strength” vector,¹ because “stronger” nodes are deemed as potential ancestors of “weaker” nodes according to the influence matrix. From this point of view, Lemma 1 recommends initiating a real-valued vector and then comparing its elements pair-wise to produce an influence matrix. Meanwhile, generating the connectivity matrix is relatively straightforward—any real-valued matrix $\mathbf{D} \in \mathbb{R}^{d \times d}$ can be

¹This is equivalent to the “potential” vector in [Yu *et al.*, 2021] and “priority score” vector in [Massidda *et al.*, 2024].

```

1 def Vec2DAG(p: np.ndarray) -> np.ndarray:
2     c = p[:d]                                # R^d
3     D = p[d:].reshape(d, d)                  # R^(dxd)
4
5     C = c[:, None] > c[None, :]  # C[i, j] = c[i] > c[j]
6     E = D > 0                                # E[i, j] = D[i, j] > 0
7
8     A = C * E
9     return A

```

Figure 2: Unconstrained DAG parameterization. This function takes as input a real-valued vector $\mathbf{p} \in \mathbb{R}^{d \cdot (d+1)}$ and deterministically transforms it into an adjacency matrix of a d -node DAG.

masked at a fixed threshold, which we choose 0 for simplicity, to yield a connectivity matrix:

$$E_{ij} = \begin{cases} 1 & \text{if } D_{ij} > 0 \\ 0 & \text{otherwise} \end{cases} \quad (8)$$

By concatenating the “node strength” vector $\mathbf{c} \in \mathbb{R}^d$ and the flattened “edge strength” matrix $\mathbf{D} \in \mathbb{R}^{d \times d}$ into one vector, we have a representation $\mathbf{p} \in \mathbb{R}^{d \cdot (d+1)}$ that can uniquely identifies any DAG. As a result, to generate a DAG we can simply draw a vector \mathbf{p} then convert it into the respective DAG by plugging Eqn. (7) and Eqn. (8) into Eqn. (6). This procedure, denoted as $\mathbf{A} = \text{Vec2DAG}(\mathbf{p})$, is depicted in Figure 1 and can be implemented in a few lines of code, as illustrated in Figure 2.

Notably, this approach can generate a valid DAG in a single step since sampling \mathbf{p} can be done instantly in an unconstrained manner, and merely costs $\mathcal{O}(d^2)$ parallelizable operations compared with the $\mathcal{O}(d^3)$ cost of ordering generation using Gumbel-Sinkhorn [Cundy *et al.*, 2021; Charpentier *et al.*, 2022] and multiple-step RL methods [Wang *et al.*, 2021; Yang *et al.*, 2023b,a]. Moreover, our generation technique is one-step, and thus does not require learning any transition function, which vastly reduces the computational burden compared with RL methods based on sequential decisions.

3.2 Reinforcement Learning for DAG Search

Policy and Action. Utilizing RL, we seek for a policy π that outputs a continuous action $\mathbf{p} \in \mathbb{R}^{d \cdot (d+1)}$, which is the parameter space of DAGs of d nodes. In this work, we consider stochastic policies for better exploration, i.e., we parametrize our policy by an isotropic Gaussian distribution with learnable means and variances: $\pi_\theta(\mathbf{p}) = \mathcal{N}(\mathbf{p}; \mu_\theta, \text{diag}(\sigma_\theta^2))$. Since our policy generates a DAG representation in just one step, every trajectory starts with the same initial state and terminates after only one transition, so the attention on states and transitions can be lifted in our method.

Reward. As we aim to minimize the graph score, the reward of an action in our method is set as the negated graph score of the DAG induced by that action: $\mathcal{R}(\mathbf{p}) = -\mathcal{S}(\mathcal{D}, \text{Vec2DAG}(\mathbf{p}))$. In our experiments, we use the BIC score similarly to Zhu *et al.* [2020]; Wang *et al.* [2021]; Yang *et al.* [2023a], where linear regression is used for linear data and Gaussian process regression is adopted for nonlin-

Algorithm 1 REACT method for causal discovery.

Input: Dataset $\mathcal{D} = \{\mathbf{x}^{(k)}\}_{k=1}^n \in \mathbb{R}^{n \times d}$, score function $\mathcal{S}(\mathcal{D}, \cdot)$, batch size B , and learning rate η .

Output: Estimated causal DAG $\hat{\mathcal{G}}$.

1: Create environments with score function \mathcal{S} . \triangleright Sec. 3.2

2: Initialize policy $\pi_\theta(\cdot)$.

3: **while** not terminated **do**

4: Draw a minibatch of B actions from the policy: $\{\mathbf{p}^{(k)} \sim \pi_\theta\}_{k=1}^B$.

5: Collect rewards $\{r^{(k)}\}_{k=1}^B$ according to the drawn actions from the environments.

6: Update policy as \triangleright Sec. 3.2

$$\nabla_\theta \mathcal{J} := \frac{1}{B} \sum_{k=1}^B \nabla_\theta \ln \pi_\theta(\mathbf{p}^{(k)}) \cdot r^{(k)}$$

$$\theta := \theta + \eta \nabla_\theta \mathcal{J}$$

7: **end while**

8: Sample an action from the learned policy: $\mathbf{p} \sim \pi_\theta$.

9: $\hat{\mathcal{G}} := \text{Vec2DAG}(\mathbf{p})$. \triangleright Sec. 3.1

10: Post-process $\hat{\mathcal{G}}$ by pruning if needed. \triangleright Sec. 3.3

11: **return** $\hat{\mathcal{G}}$.

ear data. That being said, any valid scoring and regression method can be seamlessly integrated to our method.

Policy Gradient Algorithm. Since our action space is continuous, we employ policy gradient methods, which are well established for handling continuous actions. The training objective is to maximize the expected return defined as $\mathcal{J}(\theta) = \mathbb{E}_{\mathbf{p} \sim \pi_\theta} [\mathcal{R}(\mathbf{p})]$. The differential entropy of the policy can also be added as a regularization term to encourage exploration [Mnih *et al.*, 2016], however we find in our experiments that the stochasticity offered by the policy suffices for exploration. That said, we also investigate the effect of entropy regularization in our empirical studies. During training, the parameter θ is updated in the direction suggested by the policy gradient as given by the policy gradient theorem [Sutton *et al.*, 1999]:

$$\nabla_\theta \mathcal{J}(\theta) = \mathbb{E}_{\mathbf{p} \sim \pi_\theta(\mathbf{p})} [\nabla_\theta \ln \pi_\theta(\mathbf{p}) \cdot \mathcal{R}(\mathbf{p})]. \quad (9)$$

Note that since our trajectories are one-step and our environment is deterministic, the state-action value function is always equal to the immediate reward, and therefore there is no need for a critic to estimate the value function. Hence, vanilla policy gradient works well out-of-the-box for our framework, yet in practice our method can be implemented with more advanced algorithms for improved training efficiency. In addition, while policy gradient only ensures local convergence under suitable conditions [Sutton *et al.*, 1999], our empirical evidences remark that our method can reach the exact ground truth DAG in notably many cases.

3.3 Post Processing

The edges penalty term in the BIC score in Eqn. (2) and Eqn. (3) does not necessarily punish denser graphs, unless the introduction of more edges degrades the score due to, for

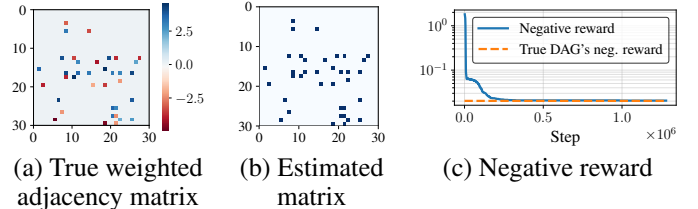


Figure 3: Learning curve of the proposed REACT method on a linear-Gaussian dataset with 30 nodes, 37 edges, and 1,000 samples. The model is trained for 1,280,000 steps (64 environments \times 20,000 steps each), which takes around 8 minutes and results in the exact ground truth DAG.

example, the curse of dimensionality. In fact, denser graphs with a slight improvement in likelihood are still preferred given sufficiently large samples, since the weight ratio between the edges count and log-likelihood terms in Eqn. (2) and Eqn. (3) is roughly $\ln(n)/n$, which tends to 0 as $n \rightarrow +\infty$. Therefore, the resultant graphs should be furthermore pruned to suppress the false discovery rate. One approach towards this end is greedily removing edges that result in non-substantial degradations in the score function. For linear models, we can simply threshold the absolute values of the estimated weights at a certain level. Alternatively, the popular CAM pruning method [Bühlmann *et al.*, 2014] can be employed for generalized additive models.

An orthogonal approach is by increasing the regularization strength on the number of edges to encourage sparsity during the learning process. However, it is non-trivial how much should be added to the penalty, which has a decisive influence onto the learning process since a strong regularization will result in many missing edges. Therefore, our method is guided by related studies [Zhu *et al.*, 2020; Wang *et al.*, 2021; Yang *et al.*, 2023a] to resort to pruning as the means to reduce extra edges. To summarize, Algorithm 1 highlights the key steps of our REACT method.

4 Numerical Evaluations

4.1 Experiment Setup

We conduct extensive empirical evaluations on both simulated and real datasets, where the ground truth DAGs are available, to compare the efficiency of the proposed REACT method with several well-established state-of-the-arts in causal discovery, including the classical algorithms PC [Spirtes *et al.*, 2000] and GES [Chickering, 2002], the popular continuous optimization approaches NOTEARS [Zheng *et al.*, 2018] and GOLEM [Ng *et al.*, 2020], and three RL-based methods RL-BIC [Zhu *et al.*, 2020], CORL [Wang *et al.*, 2021], and RCL-OG [Yang *et al.*, 2023a]. Additional implementation details are presented in Appendix C.2.

The estimated graphs are validated against ground truth DAGs on multiple evaluation metrics, including the commonly employed Structural Hamming Distance (SHD, lower is better), False Detection Rate (FDR, lower is better), True Positive Rate (TPR, higher is better), F_1 score (higher is better). The explanations of the employed metrics are provided in Appendix C.3.

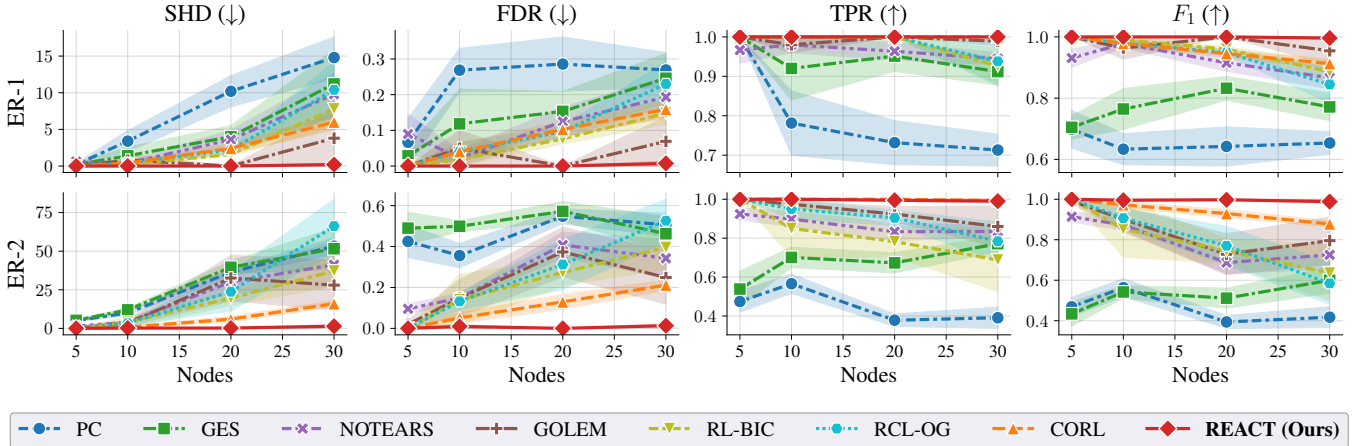


Figure 4: Causal Discovery Performance on Linear-Gaussian Data. ER-1 and ER-2 denote Erdős-Rényi graph models with expected in-degrees of 1 and 2, respectively. We compare the proposed **REACT** method with PC [Spirtes *et al.*, 2000], GES [Chickering, 2002], NOTEARS [Zheng *et al.*, 2018], GOLEM [Ng *et al.*, 2020], RL-BIC [Zhu *et al.*, 2020], CORL [Wang *et al.*, 2021], and RCL-OG [Yang *et al.*, 2023a]. The performance metrics are Structural Hamming Distance (SHD), False Detection Rate (FDR), True Positive Rate (TPR), and F_1 score. Lower SHD and FDR values are preferable, while higher values are better for TPR and F_1 . Shaded areas depict standard errors over 5 independent runs.

4.2 Linear-Gaussian Data

We first validate our proposed **REACT** method on the simplest class of causal models—linear models with Gaussian noises—in conjunction with Erdős-Rényi graph models [Erdős and Rényi, 1960] of different in-degrees, denoted as ER- k , $k \in \mathbb{N}^+$. The detailed specifications of synthetic data generation are provided Appendix C.1. Additionally, in this setting, we apply the same pruning procedure with linear regression coefficients thresholded at 0.3 for NOTEARS, RL-BIC, CORL, RCL-OG, GOLEM, as well as our method. We also use the equal-variance BIC score in Eqn. (3) for GOLEM, RL-BIC, CORL, RCL-OG, and **REACT**.

Figure 3 preliminarily demonstrates the learnability of the proposed method **REACT**, signifying that our method can reach the optimal score corresponding to the ground truth DAG fairly fast. In what follows, we report the performance of the proposed method compared against the prominent baselines for varying graph scales and sparsities in Figure 4. Our method consistently achieves near-perfect performance in all metrics with minor fluctuations for all graph sizes and densities, which can be expected thanks to its ability to explore the DAG space competently. On the other hand, it can be observed that while RL-BIC, CORL, and RCL-OG all achieve zero SHD for small graphs, i.e., 5 nodes, in both ER-1 and ER-2 models, their performance quickly deteriorates for larger graphs with exponentially increasing difficulties, especially in the harder cases of denser graphs. Overall, according to all four metrics, the runner-up method on ER-1 graphs is GOLEM, which is an algorithm specifically designed for sparse linear DAGs, while the second-best method for denser graphs ER-2 is CORL. Notably, GOLEM and CORL’s TPR are competitive with our method at nearly 1 everywhere, but their FDR clearly increases over time, suggesting that they tend to produce more spurious edges as the graph grows larger.

While it is expected that GOLEM can unlikely find the global solution due to the non-convexity of its loss function, CORL should not make such many redundant mistakes as observed due to the exploration ability of RL. We hypothesize that the curse of dimensionality is primarily responsible for the degradation of CORL, since the processes of calculating rewards and pruning in their method involve fitting many functions with high-dimensional inputs, such as regressing the last element of the causal ordering onto the first $d - 1$ elements to calculate BIC. This may introduce high variances in the reward estimates and prevent reaching the optimal policy, especially for large graphs or high-variance data like in our experiment. Conversely, our method only fits functions of the potential parents of a node, which are usually low-dimensional regression problems and thus does not suffer as much from the curse of dimensionality. Indeed, we also show in Table 4 of Appendix D.1 that our method is still able to outperform all other baselines for much denser graphs that force our method to perform higher-dimensional regressions more frequently. Even though these scenarios render our method susceptible to the curse of dimensionality—as evidenced by the higher SHD compared with sparser graphs—the empirical results reveal that our performance degradation is indeed much less severe than ordering-based methods.

4.3 Nonlinear Data with Gaussian Processes

In this section, we answer the question of whether our method can operate beyond the standard linear-Gaussian setting. To proceed, we consider more complex data generation processes involving nonlinear causal mechanisms. Particularly, following the evaluations in [Zhu *et al.*, 2020; Wang *et al.*, 2021], each causal mechanism f_i in this model is sampled from a Gaussian process with an RBF kernel of unit bandwidth, and the noises follow normal distributions with different variances, which are sampled uniformly. We evaluate the performance of the proposed method **REACT** with com-

Table 2: Causal discovery performance on nonlinear data with Gaussian processes. The data is generated with 10-node 40-edge graphs and Gaussian processes as causal mechanisms. The performance metrics are Structural Hamming Distance (SHD), False Detection Rate (FDR), and True Positive Rate (TPR). Lower SHD and FDR values are preferable, while higher values are better for TPR. The numbers are *mean \pm standard deviation* over 5 independent runs. The figures for RL-BIC are as originally reported.

Method	SHD (\downarrow)	FDR (\downarrow)	TPR (\uparrow)
PC [Spirtes <i>et al.</i> , 2000]	31.8 \pm 2.6	0.52 \pm 0.15	0.22 \pm 0.07
GES [Chickering, 2002]	29.8 \pm 5.4	0.47 \pm 0.25	0.31 \pm 0.12
NOTEARS [Zheng <i>et al.</i> , 2018]	38.0 \pm 2.2	0.59 \pm 0.24	0.06 \pm 0.04
GOLEM [Ng <i>et al.</i> , 2020]	38.8 \pm 2.9	0.66 \pm 0.23	0.05 \pm 0.02
RL-BIC [Zhu <i>et al.</i> , 2020]	6.2 \pm 1.3	0.14 \pm 0.03	0.96 \pm 0.03
CORL [Wang <i>et al.</i> , 2021]	8.4 \pm 3.9	0.19 \pm 0.09	0.91 \pm 0.08
RCL-OG [Yang <i>et al.</i> , 2023a]	6.8 \pm 0.8	0.15 \pm 0.06	0.94 \pm 0.02
REACT (Ours)	4.2 \pm 1.9	0.09 \pm 0.04	1.00 \pm 0.00

Table 3: Causal discovery performance on real-world flow cytometry data [Sachs *et al.*, 2005] with 11 nodes, 17 edges, and 853 samples. Running time is compared among RL-based methods. The figures for RL-BIC and CORL are as originally reported.

Method	Total edges	Correct edges (\uparrow)	SHD (\downarrow)	Minutes (\downarrow)
PC [Spirtes <i>et al.</i> , 2000]	8	6	11	-
GES [Chickering, 2002]	8	6	11	-
NOTEARS [Zheng <i>et al.</i> , 2018]	14	6	12	-
GOLEM [Ng <i>et al.</i> , 2020]	3	1	16	-
RL-BIC [Zhu <i>et al.</i> , 2020]	10	7	11	13
CORL [Wang <i>et al.</i> , 2021]	-	-	11	34
RCL-OG [Yang <i>et al.</i> , 2023a]	9	5	13	15
REACT (Ours)	10	7	11	7

petitors on the exact 5 datasets used by Zhu *et al.* [2020] in their experiment. We also follow Zhu *et al.* [2020]; Wang *et al.* [2021] to standardize data and apply Gaussian process regression with the median kernel bandwidth heuristic to calculate the BIC with non-equal variances according to Eqn. (2) for RL-BIC, CORL, RCL-OG, and our **REACT** method.

The empirical results reported in Table 2 verify the effectiveness of our method even on nonlinear data. Our method achieves the lowest SHD and FDR with an absolute TPR, indicating that it recovers all true edges with a few extra edges, but misses no edges. Following closely by our method is the other RL-based methods, while the remaining baselines perform poorly, which may be due to the specific emphasis on linear data in their implementations.

4.4 Real Data

Next, to confirm the validity of our method past synthetic data, we evaluate it on the prevalent real-world benchmark for causal discovery—the flow cytometry dataset [Sachs *et al.*, 2005], which involves a protein signaling network based on expression levels of proteins and phospholipids. It is comprised of both observational and interventional portions, but since our method only considers observational data, we employ the corresponding partition of the dataset with 853 samples, 11 nodes, and 17 edges.

We apply the same configurations from the nonlinear experiment to this analysis for all methods. We also employ CAM pruning [Bühlmann *et al.*, 2014] with a significance level of 0.001 to discard redundant edges for RL-BIC, CORL,

RCL-OG, and **REACT**, as suggested by Zhu *et al.* [2020]. The empirical results are provided in Table 3, showing that our method **REACT** both achieves the best SHD and number of correct edges, as well as running time among all RL-based approaches. Compared to RL-BIC, which also output graphs in a one-step policy, our proposed method does not have to evaluate the DAG regularization term for reward calculation, thus enjoying nearly a half of reduced runtime. Meanwhile, CORL and RCL-OG, being ordering-based methods with multiple-step policies, are significantly slower than our method but still cannot surpass it. Even though RCL-OG is more than two times faster than CORL, it is both slower and less accurate than our **REACT**.

4.5 Ablation Studies

Finally, we demonstrate the stability of our method against different choices of hyperparameters. In Table 6 of Appendix D.2 we examine different values for the most influential hyper-parameters of our proposed **REACT** method, including the number of training steps, number of parallel environments, learning rate, as well as entropy weight, and record the respective performance with the best baseline CORL as a reference. Overall, the figures show that our method’s performance is relatively consistent regardless of hyper-parameters, evidenced by the fact that even in the worst choices of hyper-parameters considered, **REACT** still significantly outperforms CORL in all measures. The results indicate that our method already surpasses CORL using merely 1,000 training steps per environment—10 times fewer than that of CORL, and with only 5,000 steps we achieve an SHD of less than 2. Moreover, with just a slight increase in the number of parallel environments, we can reach an SHD of almost zero. Meanwhile, learning rate plays a relatively important role, as small changes can visibly affect both the accuracy and running time of our method. Lastly, a small amount of entropy regularization can help boost exploration to achieve much better accuracies, but stronger weights immediately impacts running time and injects noises to the predictions.

5 Conclusion

In this study, a novel causal discovery method based on RL is proposed. With the introduction of a new DAG characterization that bridges an unconstrained continuous space to the constrained DAG space, we devise an RL policy that can generate DAGs efficiently without any enforcement of the acyclicity constraint, which helps improve the search for the optimal score drastically. Experiments on a wide array of both synthetic and real datasets confirm the effectiveness of our method compared with state-of-the-art baselines. In the future, many promising development directions are possible, including the adaptation of our method to more intriguing settings like causal discovery with interventional data and hidden variables, or the employment of more sophisticated RL techniques to further improve the convergence speed of our method. In addition, the action space can also be reduced to accommodate higher-dimensional data.

References

Emmanuel Bengio, Moksh Jain, Maksym Korablyov, Doina Precup, and Yoshua Bengio. Flow network based generative models for non-iterative diverse candidate generation. In *Advances in Neural Information Processing Systems*, pages 27381–27394, 2021.

Yoshua Bengio, Salem Lahlou, Tristan Deleu, Edward J Hu, Mo Tiwari, and Emmanuel Bengio. Gflownet foundations. *Journal of Machine Learning Research*, pages 1–55, 2023.

Peter Bühlmann, Jonas Peters, and Jan Ernest. Cam: Causal additive models, high-dimensional order search and penalized regression. *The Annals of Statistics*, 42:2526–2556, 2014.

Yinan Cao, Christopher Summerfield, Hame Park, Bruno Lucio Giordano, and Christoph Kayser. Causal inference in the multisensory brain. *Neuron*, 102:1076–1087, 2019.

Bertrand Charpentier, Simon Kibler, and Stephan Günemann. Differentiable dag sampling. In *Proceedings of the International Conference on Learning Representations*, 2022.

David Maxwell Chickering. Learning Bayesian networks is NP-complete. *Learning from data: Artificial intelligence and statistics V*, pages 121–130, 1996.

David Maxwell Chickering. Optimal structure identification with greedy search. *Journal of Machine Learning Research*, 3:507–554, 2002.

Diego Colombo, Marloes H Maathuis, Markus Kalisch, and Thomas S Richardson. Learning high-dimensional directed acyclic graphs with latent and selection variables. *The Annals of Statistics*, pages 294–321, 2012.

Chris Cundy, Aditya Grover, and Stefano Ermon. Bcd nets: Scalable variational approaches for Bayesian causal discovery. In *Advances in Neural Information Processing Systems*, pages 7095–7110, 2021.

Tristan Deleu, António Góis, Chris Emezue, Mansi Rankawat, Simon Lacoste-Julien, Stefan Bauer, and Yoshua Bengio. Bayesian structure learning with generative flow networks. In *Uncertainty in Artificial Intelligence*, pages 518–528, 2022.

Paul Erdős and Alfréd Rényi. On the evolution of random graphs. *Publications of the Mathematical Institute of the Hungarian Academy of Sciences*, 1960.

David Heckerman, Dan Geiger, and David M Chickering. Learning bayesian networks: The combination of knowledge and statistical data. *Machine learning*, pages 197–243, 1995.

Patrik Hoyer, Dominik Janzing, Joris M Mooij, Jonas Peters, and Bernhard Schölkopf. Nonlinear causal discovery with additive noise models. In *Advances in Neural Information Processing Systems*, 2008.

Paul Hünermund and Elias Bareinboim. Causal inference and data fusion in econometrics. *The Econometrics Journal*, page utad008, 2023.

Wouter Kool, Herke Van Hoof, and Max Welling. Stochastic beams and where to find them: The Gumbel-top-k trick for sampling sequences without replacement. In *Proceedings of the International Conference on Machine Learning*, pages 3499–3508, 2019.

Harold W Kuhn. The Hungarian method for the assignment problem. *Naval research logistics quarterly*, pages 83–97, 1955.

Hao-Chih Lee, Matteo Danieletto, Riccardo Miotto, Sarah T Cherng, and Joel T Dudley. Scaling structural learning with NO-BEARS to infer causal transcriptome networks. In *Pacific Symposium on Biocomputing*, pages 391–402, 2020.

Riccardo Massidda, Francesco Landolfi, Martina Cinquini, and Davide Bacci. Constraint-free structure learning with smooth acyclic orientations. In *Proceedings of the International Conference on Learning Representations*, 2024.

Volodymyr Mnih, Adria Puigdomenech Badia, Mehdi Mirza, Alex Graves, Timothy Lillicrap, Tim Harley, David Silver, and Koray Kavukcuoglu. Asynchronous methods for deep reinforcement learning. In *Proceedings of the International Conference on Machine Learning*, pages 1928–1937, 2016.

Ignavier Ng, AmirEmad Ghassami, and Kun Zhang. On the role of sparsity and DAG constraints for learning linear DAGs. In *Advances in Neural Information Processing Systems*, pages 17943–17954, 2020.

Jonas Peters, Joris M Mooij, Dominik Janzing, and Bernhard Schölkopf. Causal discovery with continuous additive noise models. *Journal of Machine Learning Research*, 2014.

Sebastian Prillo and Julian Eisenschlos. Softsort: A continuous relaxation for the argsort operator. In *Proceedings of the International Conference on Machine Learning*, pages 7793–7802, 2020.

Antonin Raffin, Ashley Hill, Adam Gleave, Anssi Kanervisto, Maximilian Ernestus, and Noah Dormann. Stable-baselines3: Reliable reinforcement learning implementations. *Journal of Machine Learning Research*, pages 1–8, 2021.

Aaditya Ramdas, Sashank Jakkam Reddi, Barnabás Póczos, Aarti Singh, and Larry Wasserman. On the decreasing power of kernel and distance based nonparametric hypothesis tests in high dimensions. In *Proceedings of the AAAI Conference on Artificial Intelligence*, 2015.

Joseph Ramsey, Madelyn Glymour, Ruben Sanchez-Romero, and Clark Glymour. A million variables and more: the Fast Greedy Equivalence Search algorithm for learning high-dimensional graphical causal models, with an application

to functional magnetic resonance images. *International Journal of Data Science and Analytics*, 3:121–129, 2017.

Jorma Rissanen. Modeling by shortest data description. *Automatica*, pages 465–471, 1978.

Robert W Robinson. Counting unlabeled acyclic digraphs. In *Combinatorial Mathematics V*, pages 28–43. Springer, 1977.

Karen Sachs, Omar Perez, Dana Pe’er, Douglas A Lauffenburger, and Garry P Nolan. Causal protein-signaling networks derived from multiparameter single-cell data. *Science*, 308:523–529, 2005.

Gideon Schwarz. Estimating the dimension of a model. *The Annals of Statistics*, pages 461–464, 1978.

Richard Sinkhorn. A relationship between arbitrary positive matrices and doubly stochastic matrices. *The Annals of Mathematical Statistics*, pages 876–879, 1964.

Peter Spirtes and Clark Glymour. An algorithm for fast recovery of sparse causal graphs. *Social Science Computer Review*, 9:62–72, 1991.

Peter Spirtes, Clark N Glymour, Richard Scheines, and David Heckerman. *Causation, prediction, and search*. MIT Press, 2000.

Richard S Sutton, David McAllester, Satinder Singh, and Yishay Mansour. Policy gradient methods for reinforcement learning with function approximation. In *Advances in Neural Information Processing Systems*, 1999.

Mark Towers, Jordan K. Terry, Ariel Kwiatkowski, John U. Balis, Gianluca de Cola, Tristan Deleu, Manuel Goulão, Andreas Kallinteris, Arjun KG, Markus Krimmel, Rodrigo Perez-Vicente, Andrea Pierré, Sander Schulhoff, Jun Jet Tai, Andrew Tan Jin Shen, and Omar G. Younis. Gymnasium, 2023.

Xiaoqiang Wang, Yali Du, Shengyu Zhu, Liangjun Ke, Zhitang Chen, Jianye Hao, and Jun Wang. Ordering-based causal discovery with reinforcement learning. In *Proceedings of the International Joint Conference on Artificial Intelligence*, pages 3566–3573, 2021.

Dennis Wei, Tian Gao, and Yue Yu. DAGs with No Fears: A closer look at continuous optimization for learning Bayesian networks. In *Advances in Neural Information Processing Systems*, pages 3895–3906, 2020.

Dezhi Yang, Guoxian Yu, Jun Wang, Zhengtian Wu, and Maozu Guo. Reinforcement causal structure learning on order graph. In *Proceedings of the AAAI Conference on Artificial Intelligence*, pages 10737–10744, 2023.

Dezhi Yang, Guoxian Yu, Jun Wang, Zhongmin Yan, and Maozu Guo. Causal discovery by graph attention reinforcement learning. In *Proceedings of the SIAM International Conference on Data Mining*, pages 28–36, 2023.

Yue Yu, Jie Chen, Tian Gao, and Mo Yu. DAG-GNN: DAG structure learning with graph neural networks. In *International Conference on Machine Learning*, pages 7154–7163, 2019.

Yue Yu, Tian Gao, Naiyu Yin, and Qiang Ji. DAGs with No Curl: An efficient DAG structure learning approach. In *International Conference on Machine Learning*, pages 12156–12166, 2021.

Keli Zhang, Shengyu Zhu, Marcus Kalander, Ignavier Ng, Junjian Ye, Zhitang Chen, and Lujia Pan. gCastle: A python toolbox for causal discovery. *arXiv preprint arXiv:2111.15155*, 2021.

Zhen Zhang, Ignavier Ng, Dong Gong, Yuhang Liu, Ehsan Abbasnejad, Mingming Gong, Kun Zhang, and Javen Qin-feng Shi. Truncated matrix power iteration for differentiable DAG learning. In *Advances in Neural Information Processing Systems*, pages 18390–18402, 2022.

Xun Zheng, Bryon Aragam, Pradeep Ravikumar, and Eric P. Xing. DAGs with NO TEARS: Continuous optimization for structure learning. In *Advances in Neural Information Processing Systems*, pages 9472–9483, 2018.

Xun Zheng, Chen Dan, Bryon Aragam, Pradeep Ravikumar, and Eric P. Xing. Learning sparse nonparametric DAGs. In *Proceedings of the International Conference on Artificial Intelligence and Statistics*, 2020.

Shengyu Zhu, Ignavier Ng, and Zhitang Chen. Causal discovery with reinforcement learning. In *Proceedings of the International Conference on Learning Representations*, 2020.

Appendix for “Efficient Reinforced DAG Learning without Acyclicity Constraints”

A Related Work

Constraint-based² methods like PC, FCI [Spirtes and Glymour, 1991; Spirtes *et al.*, 2000] and RFCI [Colombo *et al.*, 2012] form a prominent class of causal discovery approaches. They first exploit conditional independence relationships statistically exhibited in data via a series of hypothesis tests to recover the skeleton, which is the undirected version of the DAG, and then orient the remaining edges using probabilistic graphical rules. These methods can only identify the causal graph up to its Markov equivalent class (MEC), which contains potentially many DAGs inducing the same data. In addition, their performance heavily relies on the quality of the conditional independence tests, which can deteriorate rapidly with the number of conditioning variables [Ramdas *et al.*, 2015], rendering them unsuitable for large or dense graphs.

Score-based methods is another major class of DAG learners, where each DAG is assigned a properly defined score based on its compatibility with observed data, then the DAG learning problem becomes the optimization problem for the DAG yielding the best score. Multiple well-established scoring methods can ensure that the true DAG associates with the optimal score, such as the Bayesian information criterion (BIC, Schwarz, 1978), Bayesian Dirichlet equivalence (BDe, Heckerman *et al.*, 1995), and minimum description length (MDL, Rissanen, 1978). However, solving for the optimal DAG score is NP-hard [Chickering, 1996] in general due to the huge DAG space that scales super-exponentially with the number of nodes [Robinson, 1977] and the complex acyclicity constraint.

Combinatorial greedy search methods such as GES [Chickering, 2002] and FGES [Ramsey *et al.*, 2017] resort to greedy heuristics to reduce the search space and enforce acyclicity by adding one edge at a time after explicitly checking that it would not introduce any cycle, yet this comes at the cost of the sub-optimality of the result.

Continuous optimization methods improve upon combinatorial optimization methods in scalability by the ingenious smooth acyclicity constraint, introduced and made popular with NOTEARS [Zheng *et al.*, 2018], which turns said combinatorial optimization into a continuous optimization problem. This enables bypassing the adversary between combinatorial enumeration and scalability to allow for exploring the DAG space much more effectively, where multiple edges can be added or removed in an update. Following developments, e.g., Yu *et al.* [2019]; Lee *et al.* [2020]; Zheng *et al.* [2020]; Ng *et al.* [2020]; Yu *et al.* [2021]; Zhang *et al.* [2022]; Wei *et al.* [2020] contribute to extending and improving the soft DAG characterization in scalability and convergence. Notably, unconstrained DAG parameterizations are also proposed by Yu *et al.* [2021] and Massidda *et al.* [2024], which simplify the optimization problem from a constrained to an unconstrained problem. However, continuous optimization

²Note that the term “constraint” here largely refers to statistical constraints, such as conditional independence, while “constraint” in our method refers to the acyclicity enforcement.

methods restrict the choices of the score to be differentiable functions, which exclude many well-studied scores such as BIC, BDe, MDL, or independence-based scores [Bühlmann *et al.*, 2014]. Furthermore, because of the local heuristic nature of continuous optimization, the global optimality and the acyclicity of the solution remain unclear.

Reinforcement learning methods have emerged in recent years as the promising replacement for the greedy search heuristics discussed so far, thanks to its excellent searchability via exploration and exploitation. As the pioneer in this line of work, Zhu *et al.* [2020] introduced the first RL agent that is trained to generate high-reward graphs. To handle acyclicity, they incorporate the soft DAG constraint from Zheng *et al.* [2018] into the reward function to penalize cyclic graphs. Unfortunately, this may not discard all cycles in the solution, but also increase computational cost drastically due to the unnecessary reward calculations for non-DAGs. To mitigate this issue, subsequent studies [Wang *et al.*, 2021; Yang *et al.*, 2023b,a] turn to finding the best-scoring causal ordering instead and subsequently apply variable selection onto the result to obtain a DAG, which naturally relieves our concerns with cycles. More particularly, CORL [Wang *et al.*, 2021] is the first RL method operating on the ordering space, which defines states as incomplete permutations and actions as the element to be added next. GARL [Yang *et al.*, 2023b] is proposed to enhance ordering generation by exploiting prior structural knowledge with the help of graph attention networks. Meanwhile, RCL-OG [Yang *et al.*, 2023a] introduces a notion of order graph that drastically reduces the state space size from $\mathcal{O}(d!)$ to only $\mathcal{O}(2^d)$. It is also worth noting that the emerging generative flow networks (GFlowNet, Bengio *et al.*, 2021, 2023) offer another technique for learning (distributions of) DAGs [Deleu *et al.*, 2022], in which the generation of DAGs is also viewed as a sequential generation problem, where edges are added one-by-one with explicit exclusions of edges introducing cycles, and the transition probabilities are learned via flow matching objectives. However, the generation of these orderings and DAGs are usually formulated as a Markov decision process, in which elements are iteratively added to the structure in a multiple-step fashion, which prevents efficient concurrent DAG generations and requires learning the transition functions, which is computationally involved given the multitude of discrete state-action combinations.

B Theoretical Justifications

B.1 Proof of Theorem 1

We first notice that any strictly upper-triangular matrix $\mathbf{U} \in \{0, 1\}^{d \times d}$ can be represented as

$$\mathbf{U} = \mathbf{T} \odot \mathbf{H}, \quad (10)$$

where $\mathbf{T} \in \{0, 1\}^{d \times d}$ is a strictly upper-triangular matrix with every entry above the main diagonal being 1, and $\mathbf{H} \in \{0, 1\}^{d \times d}$ is a binary matrix where $H_{ij} = U_{ij}$ if $i < j$.

Let $f : \{1, \dots, d\} \rightarrow \{1, \dots, d\}$ be the nodes’ rearrangement map corresponding with the permutation matrix $\mathbf{\Pi}$, i.e.,

decomposition $\mathbf{A} = \mathbf{\Pi}^\top \mathbf{U} \mathbf{\Pi}$ is equivalent to $A_{ij} = U_{f(i)f(j)}$ $\forall i, j$. Combine that with (10) we have

$$A_{ij} = (\mathbf{T} \odot \mathbf{H})_{f(i)f(j)} \quad (11)$$

$$\Leftrightarrow A_{ij} = T_{f(i)f(j)} \times H_{f(i)f(j)} \quad (12)$$

$$\Leftrightarrow A_{ij} = (\mathbf{\Pi}^\top \mathbf{T} \mathbf{\Pi})_{ij} \times (\mathbf{\Pi}^\top \mathbf{H} \mathbf{\Pi})_{ij} \quad (13)$$

$$\Leftrightarrow \mathbf{A} = \underbrace{(\mathbf{\Pi}^\top \mathbf{T} \mathbf{\Pi})}_{\mathbf{C}} \odot \underbrace{(\mathbf{\Pi}^\top \mathbf{H} \mathbf{\Pi})}_{\mathbf{E}} \quad (14)$$

It can be seen that $\mathbf{C} = \mathbf{\Pi}^\top \mathbf{T} \mathbf{\Pi}$ satisfies the Definition 1 of influence matrix, and since \mathbf{H} is a square binary matrix, $\mathbf{E} = \mathbf{\Pi}^\top \mathbf{H} \mathbf{\Pi}$ is also a binary matrix and thus is a connectivity matrix, which completes our proof.

B.2 Proof of Lemma 1

Since \mathbf{C} represents a complete DAG, $C_{ij} = 1$ is equivalent to $\deg_i^+ > \deg_j^+$ where \deg^+ is the out-degree of a node in the DAG represented by \mathbf{C} . On the other hand, we also have $\deg_i^+ \neq \deg_j^+$ for all $i \neq j$ due to the completeness of \mathbf{C} . Therefore, for infinitely many strictly increasing maps $g : \mathbb{N} \rightarrow \mathbb{R}$, the choice $c_i = g(\deg_i^+)$ always satisfies Eqn. (7) since $g(\deg_i^+) > g(\deg_j^+) \Leftrightarrow \deg_i^+ > \deg_j^+ \Leftrightarrow C_{ij} = 1$, which concludes our proof.

B.3 Derivation of BIC scores

BIC is a parametric score that assumes a model for the causal mechanisms, e.g., linear-Gaussian, which comes with a set of parameters ψ . This score is used to approximate the likelihood of data given the model after marginalizing out the model parameters:

$$\ln p(\mathcal{D} | \mathcal{G}) = \ln \int p(\mathcal{D} | \psi, \mathcal{G}) p(\psi | \mathcal{G}) d\psi \approx -\frac{\mathcal{S}_{\text{BIC}}}{2}. \quad (15)$$

Given a DAG \mathcal{G} , the BIC score is defined as follows:

$$\mathcal{S}_{\text{BIC}}(\mathcal{D}, \mathcal{G}) = -2 \ln p(\mathcal{D} | \hat{\psi}, \mathcal{G}) + |\mathcal{G}| \ln n, \quad (16)$$

where $\hat{\psi}$ is the maximum-likelihood estimator of $p(\mathcal{D} | \psi, \mathcal{G})$, $|\mathcal{G}|$ is the number of edges in \mathcal{G} , and n is the number of samples in \mathcal{D} .

Non-equal variances case

Recall that the additive noise model under Gaussian noise is given by $X_i := f_i(\mathbf{X}_{\text{pa}_i}) + E_i$, where $E_i \sim \mathcal{N}(0, \sigma_i^2)$. This implies $X_i \sim \mathcal{N}(f_i(\mathbf{X}_{\text{pa}_i}), \sigma_i^2)$ and the log-likelihood of an empirical dataset $\mathcal{D} = \{\mathbf{x}^{(k)}\}_{k=1}^n$ is given by

$$\mathcal{L} = \ln p(\mathcal{D} | f, \sigma, \mathcal{G}) \quad (17)$$

$$= -\frac{1}{2} \sum_{k=1}^n \sum_{i=1}^d \frac{(x_i^{(k)} - f_i(x_{\text{pa}_i}^{(k)}))^2}{\sigma_i^2} \quad (18)$$

$$- \frac{n}{2} \sum_{i=1}^d \ln \sigma_i^2 + \text{const}, \quad (19)$$

where the constant does not depend on any variable.

The maximum likelihood estimator for f_i can be found via least square methods, and that of σ_i^2 can be found by solving $\frac{\partial \mathcal{L}}{\partial \sigma_i^2} = 0$, which yields

$$\hat{\sigma}_i^2 = \frac{1}{n} \sum_{k=1}^n \underbrace{\left(x_i^{(k)} - \hat{f}_i(x_{\text{pa}_i}^{(k)}) \right)^2}_{\text{SSR}_i}. \quad (20)$$

Plugging this back to Eqn. (17) gives

$$\hat{\mathcal{L}} = -\frac{n}{2} \sum_{i=1}^d \ln \frac{\text{SSR}_i}{n} + \text{const}. \quad (21)$$

Finally, we obtain the BIC score for the non-equal variances case by incorporating this into Eqn. (16):

$$\mathcal{S}_{\text{BIC}}(\mathcal{D}, \mathcal{G}) = n \sum_{i=1}^d \ln \frac{\text{SSR}_i}{n} + |\mathcal{G}| \ln n + \text{const}, \quad (22)$$

Equal variances case

Similarly to the unequal variances case, by assuming $\sigma_1 = \dots = \sigma_d = \sigma$, we solve for $\frac{\partial \mathcal{L}}{\partial \sigma^2} = 0$ and obtain

$$\hat{\sigma}^2 = \frac{1}{nd} \sum_{i=1}^d \sum_{k=1}^n \underbrace{\left(x_i^{(k)} - \hat{f}_i(x_{\text{pa}_i}^{(k)}) \right)^2}_{\text{SSR}_i}. \quad (23)$$

Substituting this estimate into Eqn. (17) yields us with

$$\hat{\mathcal{L}} = -\frac{nd}{2} \ln \frac{\sum_{i=1}^d \text{SSR}_i}{nd}. \quad (24)$$

For the last step, the BIC score for the equal variance case is given by substitution as

$$\mathcal{S}_{\text{BIC}}(\mathcal{D}, \mathcal{G}) = nd \ln \frac{\sum_{i=1}^d \text{SSR}_i}{nd} + |\mathcal{G}| \ln n + \text{const}. \quad (25)$$

C Additional Experiment Details

C.1 Synthetic Linear-Gaussian Data

To simulate data for a given number of nodes d , we first generate a DAG following the Erdős-Rényi graph model [Erdős and Rényi, 1960] with a random ordering and an expected in-degree of $k \in \mathbb{N}^+$, denoted by ER- k . Next, edge weights are randomly sampled from the uniform distribution $\mathcal{U}([-5, -2] \cup [2, 5])$, giving a weighted matrix $\mathbf{W} \in \mathbb{R}^{d \times d}$ where zero entries indicate no connections, then the noises are sampled from the standard Gaussian distribution $E_i \sim \mathcal{N}(0, 1)$.

Finally, we sample $n = 1,000$ observations for each dataset following the linear assignment $X_i := \sum_{j \in \text{pa}_i} W_{ji} X_j + E_i$. While linear-Gaussian models are non-identifiable in general [Spirtes *et al.*, 2000], the instances with equal noise variances adopted in this experiment are known to be fully identifiable [Peters *et al.*, 2014]. This data generation process is similar to multiple other works such as [Zheng *et al.*, 2018; Zhu *et al.*, 2020; Wang *et al.*, 2021] and is also conducted using the gCastle utility [Zhang *et al.*, 2021], except for a higher data variance with slightly more influential edge weights.

C.2 Implementation Details

Our set of baseline methods contains a wide range of both well-established and recent approaches, namely the classical algorithms PC [Spirtes *et al.*, 2000] and GES [Chickering, 2002], the popular continuous optimization approaches NOTEARS [Zheng *et al.*, 2018] and GOLEM [Ng *et al.*, 2020], and three RL-based methods RL-BIC [Zhu *et al.*, 2020], CORL [Wang *et al.*, 2021], and RCL-OG [Yang *et al.*, 2023a], where the implementations are publicly available.

Particularly, we adopt the well-established gCastle package version 1.0.3 (<https://github.com/huawei-noah/trustworthyAI>) for the implementations of all baseline methods except for RCL-OG, whose the implementation can be found at <https://www.sdu-idea.cn/codes.php?name=RCL-OG>. Note that since RCL-OG is essentially a Bayesian method, we use the best-scoring DAG from its 1,000 posterior samples as the output for a fair comparison with other methods. Default hyperparameters for each implementation are used unless specifically indicated. The detailed configurations of all methods are provided in Appendix C.4.

Our proposed **REACT** method is implemented using the Stable Baselines3 toolset [Raffin *et al.*, 2021] with the Advantage Actor Critic algorithm (A2C, Mnih *et al.*, 2016) and a custom DAG environment built on top of Gymnasium [Towers *et al.*, 2023]. We choose A2C due to its simplicity compared with other policy gradient alternatives, yet it still works really well off-the-shelf with no parameter tuning. In fact, we only set the number of environments and training steps to match those of the original RL-based method RL-BIC, while leaving all other hyper-parameters unchanged (see Appendix C.4 for more details), except for the additional use of advantage normalization for better training stability.

Experiments are executed on a mix of several machines running Ubuntu 20.04/22.04 with the matching Python environments. All running time, if available, is measured on a machine with an Intel Core i9-12900 CPU, 64GB of RAM, and Nvidia RTX 4060Ti 16GB GPU.

C.3 Metrics

The estimated graphs are assessed against ground truth DAGs on multiple evaluation metrics, including the commonly employed Structural Hamming Distance (SHD, lower is better), False Detection Rate (FDR, lower is better), True Positive Rate (TPR, higher is better), F_1 score (higher is better), and running time (lower is better) in certain cases. SHD counts the minimal number of edge additions, removals, and reversals in order to turn one graph into another. FDR is the ratio of incorrectly estimated edges over all estimated edges, while TPR is the proportion of correctly identified edges over all true edges. F_1 is calculated by treating the problem as a binary classification problem with the estimated matrix as predictions and ground truth matrix as true class labels.

In addition, due to the fact that PC and GES only learn up to the MEC of the true DAG, their estimates are complete partial DAGs that contain potentially many undirected edges, so following [Zheng *et al.*, 2018; Zhu *et al.*, 2020] we also treat them favorably by considering every unoriented edge as one correct edge whenever one of the two directions presents in the ground truth.

Table 4: Causal discovery performance on dense graphs (30-node ER-5) with linear-Gaussian data. We compare the proposed **REACT** method with PC [Spirtes *et al.*, 2000], NOTEARS [Zheng *et al.*, 2018], GOLEM [Ng *et al.*, 2020], RL-BIC [Zhu *et al.*, 2020], and CORL [Wang *et al.*, 2021]. The performance metrics are Structural Hamming Distance (SHD), False Detection Rate (FDR), and True Positive Rate (TPR). Lower SHD and FDR values are preferable, while higher values are better for TPR. The numbers are *mean* \pm *standard deviation* over 5 independent runs.

Method	SHD (\downarrow)	FDR (\downarrow)	TPR (\uparrow)
PC	169.0 ± 5.2	0.78 ± 0.04	0.11 ± 0.02
NOTEARS	157.4 ± 13.9	0.68 ± 0.11	0.09 ± 0.07
GOLEM	169.4 ± 13.1	0.73 ± 0.06	0.13 ± 0.04
RL-BIC	160.4 ± 9.1	0.72 ± 0.1	0.11 ± 0.12
CORL	131.8 ± 22.4	0.48 ± 0.06	0.79 ± 0.06
REACT (Ours)	8.8 ± 8.7	0.04 ± 0.04	0.98 ± 0.02

C.4 Hyper-parameters

In Table 5 we provide the comprehensive set of hyper-parameters for all methods in each of our experiment. The hyper-parameters not mentioned here are set with default values in the respective implementation.

D Additional Experiments

D.1 Dense Graphs

We compare the proposed **REACT** method with competitors in the linear-Gaussian setting with dense graphs, i.e., ER-5, and report the results in Table 4. In this experiment GES does not halt after 7 hours and RCL-OG encounters numerical instabilities for all datasets so we exclude them from the baselines.

D.2 Ablation Studies

In Table 6 we examine different values for the most influential hyper-parameters of the employed RL algorithm A2C, including the number of training steps, number of parallel environments, learning rate, as well as entropy weight, and record the respective performance with the best baseline CORL as a reference.

Table 5: Hyper-parameters used in our experiments. Unmentioned hyper-parameters are left unchanged.

Experiment	Linear	Nonlinear	Real
REACT (Ours)			
No. environments	64	64	64
No. steps per environment	20,000	30,000	30,000
Data normalization	No	Yes	Yes
Advantage normalization (for A2C)	Yes	Yes	Yes
Pruning	Yes (weight threshold at 0.3)	No	Yes (CAM pruning)
Scoring method	BIC Equal Variances	BIC Non-equal Variances	BIC Non-equal Variances
Regression method	Linear Regression	Gaussian Process Regression	Gaussian Process Regression
RL-BIC			
Data normalization	No		
Pruning	Yes (weight threshold at 0.3)		
Scoring method	BIC Equal Variances	Use reported results	Use reported results
Regression method	Linear Regression		
CORL			
Data normalization	No	Yes	
Pruning	Yes (weight threshold at 0.3)	No	
Scoring method	BIC Equal Variances	BIC Non-equal Variances	Use reported results
Regression method	Linear Regression	Gaussian Process Regression	
RCL-OG			
Data normalization	No	Yes	Yes
Pruning	Yes (weight threshold at 0.3)	No	Yes (CAM pruning)
Scoring method	BIC Equal Variances	BIC Non-equal Variances	BIC Non-equal Variances
Regression method	Linear Regression	Gaussian Process Regression	Gaussian Process Regression
GOLEM			
Equal Variances	Yes	No	No
λ_1	0.02	0.002	0.002

Table 6: Performance sensitivity w.r.t. hyperparameters. We study the performance of **REACT** subjected to the variations of hyperparameters. We employ linear-Gaussian datasets with 30 nodes on ER-2 graphs and use CORL as a reference. *First block*: we consider different training steps per environment. *Second block*: we examine increasing numbers of parallel environments. *Third block*: we try multiple learning rates. *Fourth block*: we study the effect of varying the entropy regularization weight. For each row, we compute the means and standard deviations over 5 independent datasets. **Bold**: best performance in each block. Unless otherwise indicated, the remaining hyperparameters are used according to Table 5 in the Appendix. Time is measured with experiments in each block running in parallel. Unless otherwise stated, we use 64 parallel environments trained for 20,000 steps each, a learning rate of 0.0007, and no entropy regularization by default.

Value	SHD (↓)	FDR (↓)	TPR (↑)	F_1 (↑)	Minutes (↓)
CORL for reference					
16	± 4.6	0.21 ± 0.06	0.99 ± 0.01	0.88 ± 0.03	90.1 ± 4
<i>Number of training steps per environment</i>					
1,000	12 ± 9.2	0.14 ± 0.1	0.96 ± 0.04	0.91 ± 0.07	8.7 ± 0.7
5,000	1.8 ± 2.4	0.02 ± 0.02	0.99 ± 0.02	0.98 ± 0.02	12.4 ± 0.9
20,000	1.4 ± 2.6	0.01 ± 0.02	0.99 ± 0.02	0.99 ± 0.02	14.1 ± 0.4
<i>Number of parallel environments</i>					
16	4.0 ± 4.8	0.05 ± 0.06	0.98 ± 0.02	0.97 ± 0.04	8.4 ± 0.7
64	1.4 ± 2.6	0.01 ± 0.02	0.99 ± 0.02	0.99 ± 0.02	14.1 ± 0.4
96	0.04 ± 0.6	0.01 ± 0.01	1.0 ± 0.01	0.99 ± 0.01	18.8 ± 0.3
<i>Learning rate</i>					
0.0003	0.2 ± 0.45	0.0 ± 0.01	1.0 ± 0.0	1.0 ± 0.0	33.1 ± 1.4
0.0007	1.4 ± 2.6	0.01 ± 0.02	0.99 ± 0.02	0.99 ± 0.02	14.1 ± 0.4
0.001	2.6 ± 5.3	0.03 ± 0.05	0.98 ± 0.04	0.98 ± 0.04	9.9 ± 0.4
<i>Entropy coefficient</i>					
0	1.4 ± 2.6	0.01 ± 0.02	0.99 ± 0.02	0.99 ± 0.02	14.1 ± 0.4
0.05	0.02 ± 0.5	0.0 ± 0.01	1.0 ± 0	1.0 ± 0	18.9 ± 3
0.1	0.8 ± 0.5	0.01 ± 0.01	1.0 ± 0	0.99 ± 0.01	56 ± 1.6